

# Antiproton Flux in Cosmic Ray Propagation Models with Anisotropic Diffusion

Phillip Grajek<sup>1</sup>, Kaoru Hagiwara<sup>1,2</sup>

<sup>1</sup> *KEK Theory Center, Tsukuba, 305-0801 Japan*

<sup>2</sup> *Sokendai, Tsukuba, 305-0801 Japan*

## Abstract

Recently a cosmic ray propagation model has been introduced, where anisotropic diffusion is used as a mechanism to allow for  $\mathcal{O}(100)$  km/s galactic winds. This model predicts a reduced antiproton background flux, suggesting an excess is being observed. We implement this model in GALPROP v50.1 and perform a  $\chi^2$  analysis for B/C,  $^{10}\text{Be}/^9\text{Be}$ , and the recent PAMELA  $\bar{p}/p$  datasets. By introducing a power-index parameter  $\alpha$  that dictates the dependence of the diffusion coefficient  $D_{xx}$  on height  $|z|$  away from the galactic plane, we confirm that isotropic diffusion models with  $\alpha = 0$  cannot accommodate high velocity convective winds suggested by ROSAT, while models with  $\alpha = 1$  ( $D_{xx} \propto |z|$ ) can give a very good fit. A fit to B/C and  $^{10}\text{Be}/^9\text{Be}$  data predicts a lower  $\bar{p}/p$  flux ratio than the PAMELA measurement at energies between approximately 2 GeV to 20 GeV. A combined fit including in addition the  $\bar{p}/p$  data is marginal, suggesting only a partial contribution to the measured antiproton flux.

## 1 Introduction

In 2008-2009, the cosmic ray (CR) observation experiments PAMELA [1] and FERMI [2] both recorded an anomalous positron flux in excess of the expected astrophysical background. Similar excesses were also reported by the ATIC [3] and HESS [4] experiments at different energies. These observations initiated a flurry of activity aimed at explaining the discrepancy. Proposed solutions include both astrophysical sources, such as local pulsars [5, 6, 7], as well as more exotic sources such as annihilating or decaying dark matter particles [8, 9, 10]. The amount to which the latter contributes is extremely important information, as many models of new physics that extend the Standard Model predict the existence of particles that can make excellent candidates for dark matter.

Inherent to any of the possible solutions is an assumption for the underlying physics describing how the CR particles are transported from their sources to Earth. At present,

our understanding of how CR propagate throughout the galaxy is mature but still incomplete. The most realistic description of CR propagation is currently obtained from models that assume CR transport occurs via a combination of spatial diffusion (resulting from interaction with the random and complicated galactic magnetic field) and convection (resulting from interaction with large-scale streaming of CR away from the galactic disk). Explicit implementations have been presented in the literature. These include both semi-analytic [11, 12] as well as fully numerical treatments [13, 14, 15, 16].

In the canonical propagation scenario, the diffusion behavior is assumed to be identical everywhere in the galaxy: both in the gaseous disk as well as the surrounding region known as the halo. This isotropic diffusion model is capable of reproducing numerous astrophysical observations well, and this has led to its adoption as the model from which astrophysical backgrounds are normally derived. However, in isotropic diffusion models the convective wind velocity is limited to no more than about 10-20 km/s. Assuming a higher wind velocity results in the incorrect prediction of several existing observations, most notably measurements of secondary-to-primary ratios such as the boron-to-carbon (B/C) ratio, as well as the ratio of radioactive beryllium isotopes ( $^{10}\text{Be}/^9\text{Be}$ ) [17, 18, 19]. These ratios, in particular, are highly sensitive to the parameters that control the various CR transport mechanisms, and are often used to benchmark predictions of a given model. While very high velocity galactic winds on the order of 1000 km/s have been observed in other galaxies [20], until recently it was thought that the Milky Way did not exhibit a wind, or that the wind velocity was limited to very low values. However, in 2007 the ROSAT satellite observed x-ray emission from within the Milky Way that is consistent with the presence of a galactic wind having a velocity of a few hundred km/s [21, 22].

The measurements are also consistent with a wind velocity profile that exhibits spatial dependence, and follows the radial distribution of supernova remnants (SNR) in the galaxy. The presence of high-velocity, radially dependent galactic winds appear to be natural and may also explain the large bulge-to-disk ratio observed by INTEGRAL [23, 24].

Recently, a propagation model has been introduced that employs both a radially dependent convective wind profile and *anisotropic* diffusion, where the diffusion behavior is not uniform throughout the galaxy, but instead varies as a function of position [25]. Specifically, the model assumes that the intensity of CR diffusion increases with distance from the galactic plane. This model is capable of supporting a convective wind velocities of several hundred km/s, which is consistent with the ROSAT measurement, while simultaneously reproducing benchmark measurements such as the B/C and  $^{10}\text{Be}/^9\text{Be}$  ratios with similar accuracy to the traditional isotropic diffusion model. A crucial prediction of this scenario is that the astrophysical anti-proton background flux appears lower than what is predicted by isotropic diffusion models [26]. Such an outcome has significant implications for the indirect detection of particle dark matter, as it would reduce constraints on models for new physics that tend to over-predict the antiproton flux, assuming no excess is currently observed in the data [27].

In this paper we implement the anisotropic propagation model of [25] in the public CR propagation code GALPROP v50.1 [14], and explore varying levels of diffusion anisotropy by adjusting the rate at which the diffusion intensity increases with distance from the galactic plane. We perform a  $\chi^2$  analysis for B/C,  $^{10}\text{Be}/^9\text{Be}$  and the recent PAMELA  $\bar{p}/p$  data and find the models that fit the data best all exhibit spatially-dependent, anisotropic

diffusion. Further, we find these models predict a  $\bar{p}/p$  flux that is significantly lower than the observed flux between 2 GeV and 20 GeV. When we attempt a combined fit including the  $\bar{p}/p$  data, we find an increase in  $\chi^2_{\min}$ , by  $\Delta\chi^2 = 35.4$  for the 23 PAMELA data points considered.

## 2 Anisotropic Diffusion

As CR propagate they scatter and diffuse via interaction with turbulent fluctuations in the galactic magnetic field. Models of CR propagation traditionally assume diffusion is isotropic throughout the propagation volume. This implies a constant density of scattering centers throughout the volume, and an abrupt transition to free space (no scattering) at the outer boundary. In this case a propagating CR experiences, for a given momentum, the same scattering mean free path in the gaseous disk as it does far into the halo. In the presence of a galactic wind flow driving CR away from the gaseous disk and into the halo, the probability for a CR particle to return to the disk drops rapidly with increasing distance into the halo, as it not only must survive the convective action of the wind, but also an increasing number of scattering events on its return trip. The interplay between diffusive scattering and convective transport strongly affects the times a CR particle spends in the gaseous disk and halo regions of the galaxy. This, in turn, affects the prediction for the CR flux at Earth. In isotropic diffusion models the convective wind speed is limited to less than approximately 20 km/s before it is no longer possible to reproduce key observations such as the B/C ratio [17, 18, 19]. This velocity limit is in conflict with measurements from the ROSAT satellite, which are consistent with galactic wind speeds up to several hundred km/s [21, 22].

In the anisotropic propagation model of [25], CR diffusion is taken to be spatially dependent, and increases monotonically with distance above the gaseous disk. This corresponds to a gradual reduction in the density of scattering centers (and a smooth transition to free space) as CR travel from the disk towards the outer boundary of the propagation volume. In this scenario, the mean scattering length *increases* with increasing distance into the halo. Therefore, a CR particle in the halo that scatters back towards the disk can travel further before experiencing its next scattering event, which is likely in a region with a higher density of scattering centers. This "trapping" mechanism induces a drift of CR particles from areas of high diffusion to areas with low diffusion, which assists in counteracting the outward convection of CR due to the galactic wind. In this way, convection velocities of several hundred km/s can be accommodated while simultaneously preserving the CR residence times in both the disk and halo required to reproduce the CR fluxes observed at Earth.

### 3 Cosmic Ray Transport Model

For our study, we utilize the CR propagation code GALPROP v50.1 [14]. GALPROP assumes that cosmic ray propagation in our galaxy is governed by the following transport equation

$$\begin{aligned} \frac{\partial \Psi}{\partial t} - q(p, \mathbf{r}, t) = & \nabla \cdot (D_{xx} \nabla - \mathbf{V}) \Psi + \frac{\partial}{\partial p} p^2 D_{pp} \frac{\partial}{\partial p} \frac{1}{p^2} \Psi \\ & - \frac{\partial}{\partial p} \left[ \dot{p} \Psi - \frac{p}{3} (\nabla \cdot \mathbf{V}) \Psi \right] \\ & - \frac{1}{\tau_f} \Psi - \frac{1}{\tau_r} \Psi \end{aligned} \quad (1)$$

where  $\Psi(p, \mathbf{r}, t)$  is the density of CR with total momentum  $p$  at location  $\mathbf{r}$  at time  $t$ . The cosmic ray source distribution, as well as contributions from nuclear spallation and

decays are included in  $q(p, \mathbf{r}, t)$ . On the RHS,  $D_{xx}$  is the spatial diffusion coefficient while  $\mathbf{V}(\mathbf{r})$  is the velocity profile of an assumed galactic wind. The term proportional to  $D_{pp}$  accounts for random, stochastic accelerations (reacceleration) that result from scattering, and is equivalent to diffusion in momentum space. The term  $p(\nabla \cdot \mathbf{V})/3$  accounts for adiabatic loss or gain in momentum, in the case that the wind velocity is location dependent. Finally, the term with  $\dot{p} \equiv dp/dt$  accounts for momentum losses such as inverse Compton scattering, bremsstrahlung, as well as synchrotron radiation, while terms with  $\tau_f^{-1}$  and  $\tau_r^{-1}$  account for losses due to fragmentation and radioactive decay, respectively. GALPROP assumes a cylindrical propagation region having maximum radius from the galactic center  $r = r_{\max}$ , and maximum extension above and below the galactic disk  $z = L$ . Free escape ( $\Psi = 0$ ) is assumed at the boundaries of the cylinder.

### 3.1 GALPROP Modifications

In this work the original GALPROP source code is modified in order to simulate anisotropic diffusion and a radially-dependent, ROSAT compatible convective wind. We follow closely the setup outlined in [25]. GALPROP utilizes the Crank-Nicholson implicit method [33] to numerically solve Eq. (1) and it is necessary to compute the finite-difference expansion coefficients in order to enact any modifications. The coefficients resulting from the inclusion of spatially dependent diffusion and convection have been computed and they agree to those in [25] in the limit of an equidistant computational grid. We assume the following grid spacing:  $\Delta r = 1$  kpc and  $\Delta z = 0.1$  kpc throughout this analysis. The propagation cylinder height  $L$  is allowed to vary, however the maximum radius is fixed at  $r_{\max} = 20$  kpc.

The spatial diffusion coefficient  $D_{xx}$  is taken to be isotropic within a slab of thickness

1 kpc above and below the galactic plane, and anisotropic at distances  $|z| \geq 1$  kpc:

$$D_{xx}(\rho) = \beta D_0 \left( \frac{\rho}{\rho_0} \right)^\delta, \quad |z| < 1 \text{ kpc}, \quad (2)$$

$$D_{xx}(\rho, z) = \beta D_0 \left( \frac{\rho}{\rho_0} \right)^\delta |z|^\alpha, \quad |z| \geq 1 \text{ kpc}, \quad (3)$$

where  $\beta \equiv v/c$ ,  $D_0$  is a constant,  $\rho$  is the particle rigidity (momentum/electric charge), and  $\delta$  is the associated power index. The reference rigidity  $\rho_0$  is set to 4 GV. We introduce a power index  $\alpha$  which governs the diffusion gradient;  $\alpha = 1$  was assumed in [25] and  $\alpha = 0$  reproduces the original GALPROP parameterization. The diffusion coefficient is related to the reacceleration coefficient  $D_{pp}$  via

$$D_{pp} D_{xx} = \frac{4}{3} \frac{p^2 v_A^2}{\delta(4 - \delta^2)(4 - \delta)} \quad (4)$$

where  $v_A$  is the speed of propagating Alfvén waves: weak disturbances in the magnetic field that contribute to turbulent scattering. For the CR source distribution we adopt the parameterization of Case and Bhattacharya [34]:

$$Q(r, z) = \left( \frac{r}{r_0} \right)^{1.69} \exp \left[ -3.33 \frac{r - r_0}{r_0} - \frac{|z|}{z_s} \right] \quad (5)$$

where  $r_0 = 8.5$  kpc is the galacto-centric distance to Earth, and  $z_s = 200$  pc. The distribution has a peak at  $r \approx 0.51 r_0$ . The galactic wind velocity is taken to be proportional to the source distribution at  $z = 0$

$$|V(r, z)| = Q(r, z = 0)(V_0 + |z| \cdot dV/dz). \quad (6)$$

We fix the constant velocity component at  $V_0 = 100$  km/s, and the gradient at  $dV/dz = 35$  km/s/kpc, which models the galactic wind velocity profile indicated by the ROSAT data. In GALPROP the galactic wind flow is one-dimensional along  $\pm \hat{z}$  and always outward from the galactic plane. The cosmic ray injection spectrum follows a power law

in momentum,  $p^{-\eta}$ . For nuclei,  $\eta = 1.8$  for rigidity  $\rho < 9$  GV, and  $\eta = 2.4$  for  $\rho > 9$  GV. Similarly, for electrons  $\eta = 1.6$  for  $\rho < 4$  GV, 2.54 for  $4 \text{ GV} \leq \rho \leq 100 \text{ GV}$ , and 5.0 for  $\rho > 100 \text{ GV}$ . We assume a constant  $X_{\text{CO}}$  factor (conversion factor from CO integrated temperature to  $\text{H}_2$  column density) of  $1.9 \times 10^{20}$ , and an H/He ratio of 0.11.

## 4 Analysis

Using these settings as a kernel, we scan parameters  $\alpha$ ,  $D_0$ ,  $v_A$ ,  $\delta$ , and  $L$  on the following grid:  $0 \leq \alpha \leq 1$  in steps of 0.2,  $4 \text{ cm}^2/\text{s} \leq D_0 \leq 6 \text{ cm}^2/\text{s}$  in steps of  $0.2 \text{ cm}^2/\text{s}$ ,  $30 \text{ km/s} \leq v_A \leq 60 \text{ km/s}$  in steps of  $2 \text{ km/s}$ ,  $0.2 \leq \delta \leq 0.5$  in steps of 0.02, and  $4 \text{ kpc} \leq L \leq 8 \text{ kpc}$  in steps of  $1 \text{ kpc}$ . For each model point  $\{\alpha, D_0, v_A, \delta, L\}$  of the scan we compute the overall  $\chi^2$  for the resulting B/C,  $^{10}\text{Be}/^9\text{Be}$ , and  $\bar{p}/p$  flux ratio curves. For our study we assume

$$\chi^2 = \sum_{j=1}^M \sum_{i=1}^{N_j} \frac{(\bar{f}_i - f_{ij})^2}{\sigma_{ij}^2} \quad (7)$$

where index  $j$  runs over all  $M$  experimental datasets, each containing  $N_j$  measurements  $f_{ij} \pm \sigma_{ij}$  ( $i = 1$  to  $N_j$ ), and  $\bar{f}_i$  is the computed flux evaluated at the specific energy of the measurement  $i$ . Flux ratios are extracted using the CPLOT routine available on the GALPROP website<sup>1</sup>. For comparison with data, the local interstellar (LIS) flux was corrected for solar modulation using the “force field” approximation [35]. We assume the following modulation potentials, for B/C,  $^{10}\text{Be}/^9\text{Be}$ , and  $\bar{p}/p$  flux ratios, respectively,  $\Phi = 300 \text{ MV}$ ,  $350 \text{ MV}$ , and  $600 \text{ MV}$ . We include the following data. For B/C: HEAO-3 [36], CREAM [37], ACE [38], and ATIC-2 [39]. For  $^{10}\text{Be}/^9\text{Be}$ : ISOMAX [40], and ACE [41]. For  $\bar{p}/p$ : PAMELA 2010 [42]. Except for the PAMELA  $\bar{p}/p$  measurements, all the

---

<sup>1</sup>[http://galprop.stanford.edu/web\\_galprop/galprop\\_home.html](http://galprop.stanford.edu/web_galprop/galprop_home.html)



data are obtained from the Galactic Cosmic Ray Database [43]. In 4 of the 23 PAMELA data points the reported uncertainty is asymmetric. For those points the larger error bar is used. No correlation among errors have been taken into account, as indicated by expression (7). Our exercise should therefore be considered as a first exploratory study of the allowed range of the parameters of the anisotropic diffusion model of CR propagation in our galaxy.

#### 4.1 Combined fit to B/C and $^{10}\text{Be}/^9\text{Be}$

We first attempt a combined fit to both the B/C and  $^{10}\text{Be}/^9\text{Be}$  datasets. We find  $\chi^2_{\text{min}}/n_{\text{dof}} = 38.3/31$  within the range of the parameter space explored. The best-fit values and corresponding  $3\sigma$  bounds for parameters  $\alpha$ ,  $D_0$ ,  $\delta$ , and  $v_A$  are given in Table 1. A bound for  $L$  is not provided because the fit does not show significant dependence on the propagation cylinder height.

Within the  $0 \leq \alpha \leq 1$  range of our scan, the  $\chi^2_{\text{min}}$  occurs at the  $\alpha = 1$  boundary. The corresponding  $3\sigma$  allowed range is  $\alpha > 0.27$ . The isotropic diffusion limit  $\alpha = 0$  is excluded at  $4\sigma$ , which confirms the finding of [25]. We remark that while our study focuses on the  $0 \leq \alpha \leq 1$  region of parameter space, a preliminary scan using a very coarse grid indicates that  $\chi^2$  increases with  $\alpha$  for  $\alpha > 1$ . A detailed examination of the  $\alpha > 1$  region is left for a future analysis.

The  $3\sigma$  allowed range of the diffusion constant  $D_0$  is  $4.3 \times 10^{28} \text{ cm}^2/\text{s} \leq D_0 \leq 5.1 \times 10^{28} \text{ cm}^2/\text{s}$ , while that of the diffusion index  $\delta$  is  $0.35 \leq \delta \leq 0.43$ . These values are consistent with previous studies involving GALPROP [44, 13] (see also [17]) and also with magneto-hydrodynamic theory, which predicts  $\delta = 1/3$  for Kolmogorov-type turbulence power spectrum, and  $\delta = 1/2$  for a Kraichnan-type spectrum. Similarly, the  $3\sigma$  range

for the Alfvén velocity  $v_A$  is  $47 \text{ km/s} \leq v_A \leq 58 \text{ km/s}$ . These values are somewhat high compared to  $v_A \simeq 30 \text{ km/s}$  obtained for models with no convective wind [13], and  $v_A \simeq 20 \text{ km/s}$  expected for the warm ionized phase of the interstellar medium [45]. This increase is due to the large velocity gradient,  $dV/dz = 35 \text{ km/s/kpc}$ , assumed for the galactic wind (6). A positive velocity gradient implies an adiabatic energy loss in response to the reduction in pressure of the CR fluid (term proportional to  $p(\nabla \cdot \mathbf{V})/3$  in Eq. (1)). The result is a redistribution of the B/C flux spectra towards lower energies. In order to reproduce the distinct peak in B/C at  $\sim 1 \text{ GeV}$ , this reduction is compensated for with increased reacceleration, which is a mechanism that shifts CR from lower energy to higher energy. From Eq. (4) this translates into larger  $D_{pp}$ , or equivalently magnetic field disturbances that propagate with larger Alfvén velocity ( $v_A$ ).

Figure 1 shows the two-parameter likelihood surfaces for transport parameters  $D_0$ ,  $\delta$ ,  $v_A$ , and  $L$  as a function of  $\alpha$ . Contours for  $\Delta\chi^2 = 2.3, 4.61, 5.99$ , and  $9.21$  are given, corresponding to the 68%, 90%, 95% and 99% confidence level regions, respectively. The best-fit model point is indicated with a red diamond. Compared to models with isotropic diffusion ( $\alpha = 0$ ), those with spatially dependent, anisotropic diffusion ( $\alpha > 0$ ) provide significantly better fits to the data. The constraint on the propagation cylinder height  $L$  (Fig. 1d) degrades with increasing  $\alpha$ . As the diffusion gradient steepens, the distance at which a CR transitions into what is effectively free space (no scattering) occurs increasingly closer to the galactic plane, and away from the assumed boundary of the propagation region at  $L$ . This reduces the sensitivity of the model to the precise value of  $L$ , which no longer defines the extent of the magnetic corona, but becomes instead a computational parameter. In isotropic models,  $L$  strongly controls the residence time of

CR in the halo, as its position determines the location of the free escape boundary.

Figure 2 shows the B/C and  $\bar{p}/p$  flux ratio curves for model points that lie within the 68 % CL region, assuming a four parameter fit ( $\Delta\chi^2 = 4.72$ ). The grey (dark) lines correspond to the local interstellar (LIS) flux, while the green (light) lines correspond to the flux after correcting for solar modulation. The B/C flux is reproduced well. However, the  $\bar{p}/p$  flux is significantly lower than the PAMELA measurement at energies between approximately 2 GeV and 20 GeV.

## 4.2 Combined fit to B/C, $^{10}\text{Be}/^9\text{Be}$ , and $\bar{p}/p$

We next attempt a combined fit to the B/C,  $^{10}\text{Be}/^9\text{Be}$ , and also the  $\bar{p}/p$  data. We observe an increase in  $\chi^2_{\text{min}}$ , by  $\Delta\chi^2 = 35.4$  for the 23 PAMELA data points considered. Figure 3 shows the 68% CL curves obtained for the combined fit in red (dark) superimposed upon the results from Fig. 2 (B/C and  $^{10}\text{Be}/^9\text{Be}$  only) in green (light). The fit to the B/C data is now degraded somewhat as the models do not reproduce well the high precision HEAO-3 data above 1 GeV. The fit to the  $\bar{p}/p$  data is marginally improved. However, an excess flux remains between approximately 2 GeV and 15 GeV.

The lower half of Table 1 gives the best-fit parameter values and corresponding  $3\sigma$  allowed range. The two-parameter likelihood surfaces are shown in Fig. 4. Models with  $\alpha > 0$  still provide the best fits to the data, however overall larger values of  $\alpha$  (steeper diffusion gradient) are required: The best fit occurs at the  $\alpha = 1$  boundary of our scan range ( $0 \leq \alpha \leq 1$ ), and the  $3\sigma$  allowed range is  $\alpha > 0.51$ . The allowed range for parameters  $D_0$ ,  $v_A$ , and  $\delta$  are now shifted to lower values relative to those obtained for the fit to B/C and  $^{10}\text{Be}/^9\text{Be}$  only, with the most pronounced reduction occurring for the Alfvén velocity. A reduction in Alfvén velocity corresponds to weakening of the

reacceleration mechanism (smaller  $D_{pp}$  in (4)), a process that boosts CR momentum to higher values. Weaker reacceleration causes both the B/C and  $\bar{p}/p$  flux distributions to shift to lower energies, which improves the fit to  $\bar{p}/p$  but simultaneously degrades the fit to B/C. Lower values for  $D_0$  and  $\delta$  reduce the intensity of spatial diffusion, which forces CR to remain longer in the gaseous disk. This increases the rate of secondary production and boosts the B/C flux, which helps to compensate for the reduction in Alfvén velocity.

## 5 Conclusions

We consider the anisotropic propagation model of [25], which assumes that CR diffusion increases linearly with distance from the galactic disk, and radially dependent convective wind flows with maximum velocity of  $\mathcal{O}(100)$  km/s suggested by the ROSAT measurement. This model is capable of reproducing key observations such as the B/C and Be/Be flux ratios, whereas traditional models based on isotropic diffusion cannot support convective wind velocities of more than approximately 20 km/s.

We implement this model in GALPROP, and introduce a new parameter,  $\alpha$ , which controls the dependence of the diffusion coefficient  $D_{xx}$  on the distance  $|z|$  above the gaseous disk;  $\alpha = 0$  corresponding to isotropic diffusion, while  $\alpha = 1$  a linear increase as in [25]. We then perform a  $\chi^2$  analysis for the B/C,  $^{10}\text{Be}/^9\text{Be}$ , and the recent PAMELA  $\bar{p}/p$  data sets in order to constrain the transport parameters. For a combined fit to the B/C and  $^{10}\text{Be}/^9\text{Be}$  flux only, we observe  $\chi^2_{\text{min}}/n_{\text{dof}} = 38.3/31$ , indicating a good fit to both data sets. We find  $\alpha > 0.27$ ,  $4.3 \times 10^{28} \text{ cm}^2/\text{s} \leq D_0 \leq 5.1 \times 10^{28} \text{ cm}^2/\text{s}$ ,  $0.35 \leq \delta \leq 0.43$ , and  $47 \text{ km/s} \leq v_A \leq 58 \text{ km/s}$  at  $3\sigma$  for the range of parameter space we explored. The Alfvén velocity is higher than expected, and due to a large wind velocity gradient,

$dV/dz = 35 \text{ km/s/kpc}$ , required to model the wind profile suggested by the ROSAT measurements. The isotropic diffusion case  $\alpha = 0$  is excluded at  $4\sigma$ . Models within the 68% CL region predict a lower  $\bar{p}/p$  flux than the PAMELA observation between 2 GeV to 20 GeV. For a combined fit to B/C,  $^{10}\text{Be}/^9\text{Be}$  and also the PAMELA  $\bar{p}/p$  data we observe an increase in  $\chi_{\text{min}}^2$ , by  $\Delta\chi^2 = 35.4$  for the additional 23 PAMELA data points considered, indicating the overall fit is marginal. In this case we find  $\alpha > 0.51$ ,  $4.1 \times 10^{28} \text{ cm}^2/\text{s} \leq D_0 \leq 4.8 \times 10^{28} \text{ cm}^2/\text{s}$ ,  $0.33 \leq \delta \leq 0.38$ , and  $43 \text{ km/s} \leq v_A \leq 49 \text{ km/s}$  at  $3\sigma$ , which are consistent with expectations. Models within the 68% CL region give an improved fit to the  $\bar{p}/p$  flux, however the predicted distributions are still below the PAMELA observation between approximately 2 GeV to 15 GeV.

These results suggest that spatially dependent diffusion represents a viable solution to the problem of accommodating  $\mathcal{O}(100) \text{ km/s}$  convective wind flows in models of CR propagation, and that in this case the observed antiproton flux may exhibit an excess above the astrophysical background. An anomalous excess in the antiproton flux would have many implications for the indirect detection of particle dark matter (DM). For example, pair annihilation of light neutralino DM can explain the positron excess observed by e.g. PAMELA [46]. These annihilations necessarily produce hadrons in addition to leptons, and so a contribution to the antiproton flux is also expected from this scenario.

## References

- [1] O. Adriani *et al.* [PAMELA Collaboration], arXiv:0810.4995 [astro-ph].
- [2] A. A. Abdo *et al.* [The Fermi LAT Collaboration], Phys. Rev. Lett. **102**, 181101 (2009) [arXiv:0905.0025 [astro-ph.HE]].

- [3] J. Chang *et al.*, Nature **456** (2008) 362.
- [4] F. Aharonian *et al.* [H.E.S.S. Collaboration], Astron. Astrophys. **508**, 561 (2009)  
[arXiv:0905.0105 [astro-ph.HE]].
- [5] D. Hooper, P. Blasi and P. D. Serpico, JCAP **0901**, 025 (2009) [arXiv:0810.1527  
[astro-ph]].
- [6] Y. Fujita, K. Kohri, R. Yamazaki, K. Ioka, Phys. Rev. **D80**, 063003 (2009).  
[arXiv:0903.5298 [astro-ph.HE]].
- [7] S. Profumo, [arXiv:0812.4457 [astro-ph]].
- [8] J. L. Feng, [arXiv:1003.0904 [astro-ph.CO]].
- [9] K. Ishiwata, S. Matsumoto, T. Moroi, [arXiv:1008.3636 [hep-ph]].
- [10] A. Ibarra, D. Tran, JCAP **0902**, 021 (2009). [arXiv:0811.1555 [hep-ph]].
- [11] A. Putze, L. Derome, D. Maurin, Astron. Astrophys. **516**, A66 (2010).  
[arXiv:1001.0551 [astro-ph.HE]].
- [12] D. Maurin, F. Donato, R. Taillet and P. Salati, Astrophys. J. **555**, 585 (2001)  
[arXiv:astro-ph/0101231].
- [13] A. W. Strong and I. V. Moskalenko, Astrophys. J. **509**, 212 (1998)  
[arXiv:astro-ph/9807150].
- [14] A. W. Strong, I. V. Moskalenko, T. A. Porter *et al.*, [arXiv:0907.0559 [astro-ph.HE]].
- [15] C. Evoli, D. Gaggero, D. Grasso and L. Maccione, JCAP **0810**, 018 (2008)  
[arXiv:0807.4730 [astro-ph]].
- [16] G. Di Bernardo, C. Evoli, D. Gaggero *et al.*, Astropart. Phys. **34**, 274-283 (2010).  
[arXiv:0909.4548 [astro-ph.HE]].

- [17] A. W. Strong, I. V. Moskalenko and V. S. Ptuskin, *Ann. Rev. Nucl. Part. Sci.* **57**, 285 (2007) [arXiv:astro-ph/0701517].
- [18] D. Maurin, R. Taillet and F. Donato, *Astron. Astrophys.* **394**, 1039 (2002) [arXiv:astro-ph/0206286].
- [19] F. C. Jones, A. Lukasiak, V. Ptuskin, W. Webber, *Astrophys J.* **547**, 264 (2001)
- [20] S. Veilleux, G. Cecil and J. Bland-Hawthorn, *Ann. Rev. Astron. Astrophys.* **43**, 769 (2005) [arXiv:astro-ph/0504435].
- [21] D. Breitschwerdt, *Nature* **452**, 826 (2008)
- [22] J. E. Everett, *et al.*, *Astrophys J.* **674**, 258 (2007)
- [23] J. Knodlseder, *et al.*, *A&A* **441**, 513 (2005)
- [24] G. Weidenspointner, *et al.* *ESA Special Publication* **622**, 25 (2007)
- [25] I. Gebauer and W. de Boer, arXiv:0910.2027 [astro-ph.GA].
- [26] W. de Boer, *AIP Conf. Proc.* **1200**, 165 (2010) [arXiv:0910.2601 [astro-ph.CO]].
- [27] F. Donato, D. Maurin, P. Brun, T. Delahaye and P. Salati, *Phys. Rev. Lett.* **102**, 071301 (2009) [arXiv:0810.5292 [astro-ph]].
- [28] V.S. Berezhinski, S.V. Bulanov, V.A. Dogiel, V.L. Ginzburg, V.S. Ptuskin, *Astrophysics of Cosmic Rays*, North Holland, Amsterdam (2009)
- [29] I. N. Toptygin, (*Kosmicheskie Luchi v Mezplanetnykh Magnitnykh Poliakh*, Moscow, Izdatel'stvo Nauka, 1983) D. Dordrecht, Reidel Publishing Co., **387** (1985) p. Translation. Previously cited in issue 01, p. 118, Accession no. A84-10472
- [30] V. S. Ptuskin, S. I. Rogovaya, V. N. Zirakashvili, L. G. Chuvilgin, G. B. Khristiansen, E. G. Klepach, G. V. Kulikov, *Astron. Astrophys* **268**, 726 (1993)

- [31] T. Shibata, M. Hareyama, M. Nakazawa, C. Saito, *Astrophys. J.* **612**, 238 (2004)
- [32] A. W. Strong, I. V. Moskalenko and O. Reimer, *Astrophys. J.* **537**, 763 (2000)  
[Erratum-ibid. **541**, 1109 (2000)] [arXiv:astro-ph/9811296].
- [33] W. H. Press, *et al.*, *Numerical Recipes in FORTRAN* (2nd ed.; Cambridge: Cambridge Univ. Press), (1992)
- [34] G. L. Case, D. Bhattacharya, *ApJ* **504**, 761 (1998)
- [35] L. J. Gleeson and W. I. Axford, *ApJ*, **154**, 1011 (1968)
- [36] J. J. Engelmann, P. Ferrando, A. Soutoul, P. Goret and E. Juliusson, *Astron. Astrophys.* **233**, 96 (1990).
- [37] H. S. Ahn, *et al.*, *Astroparticle Physics* **30**, 133 (2008)
- [38] A. J. Davis, *et al.*, *Acceleration and Transport of Energetic Particles Observed in the Heliosphere: ACE 2000 Symposium* **528**, 421 (2000)
- [39] A. D. Panov *et al.*, arXiv:0707.4415 [astro-ph].
- [40] T. Hams *et al.*, *Astrophys. J.* **611**, 892 (2004).
- [41] N. E. Yanasak, *et al.*, *ApJ* **563**, 768 (2001)
- [42] O. Adriani *et al.* [PAMELA Collaboration], arXiv:1007.0821 [astro-ph.HE].
- [43] A. W. Strong and I. V. Moskalenko, arXiv:0907.0565 [astro-ph.HE].
- [44] A. M. Lionetto, A. Morselli and V. Zdravkovic, *JCAP* **0509**, 010 (2005)  
[arXiv:astro-ph/0502406].
- [45] E. S. Seo, V. S. Ptuskin, *ApJ*, **431**, 705 (1994)
- [46] P. Grajek, G.L. Kane, D.J. Phalen, A. Pierce, S. Watson, *Phys. Rev.* **D79**, 043506 (2009). [arXiv:0812.4555 [hep-ph]].



Combined Fit	Parameter	Best Fit Value	$3\sigma$ Range
B/C, $^{10}\text{Be}/^9\text{Be}$	$\alpha$	1.0	$> 0.27$
	$D_0$	$4.6 \times 10^{28} \text{ cm}^2/\text{s}$	$4.3 - 5.1 \times 10^{28} \text{ cm}^2/\text{s}$
	$v_A$	52 km/s	47 - 58 km/s
	$\delta$	0.38	0.35 - 0.43
B/C, $^{10}\text{Be}/^9\text{Be}$ , $\bar{p}/p$	$\alpha$	1.0	$> 0.51$
	$D_0$	$4.4 \times 10^{28} \text{ cm}^2/\text{s}$	$4.1 - 4.8 \times 10^{28} \text{ cm}^2/\text{s}$
	$v_A$	46 km/s	43 - 49 km/s
	$\delta$	0.36	0.33 - 0.38

Table 1: Best-fit model parameters for the combined  $\chi^2$  fits explored in this study. The  $3\sigma$  allowed range is given for  $L = 5$  kpc for the fit to B/C and  $^{10}\text{Be}/^9\text{Be}$  (above), and for  $L = 6$  kpc for the fit including  $\bar{p}/p$  (bottom), where we find the minimum  $\chi^2$ . No bound is provided for parameter  $L$ , as the fit does not exhibit strong dependence on the propagation cylinder height.

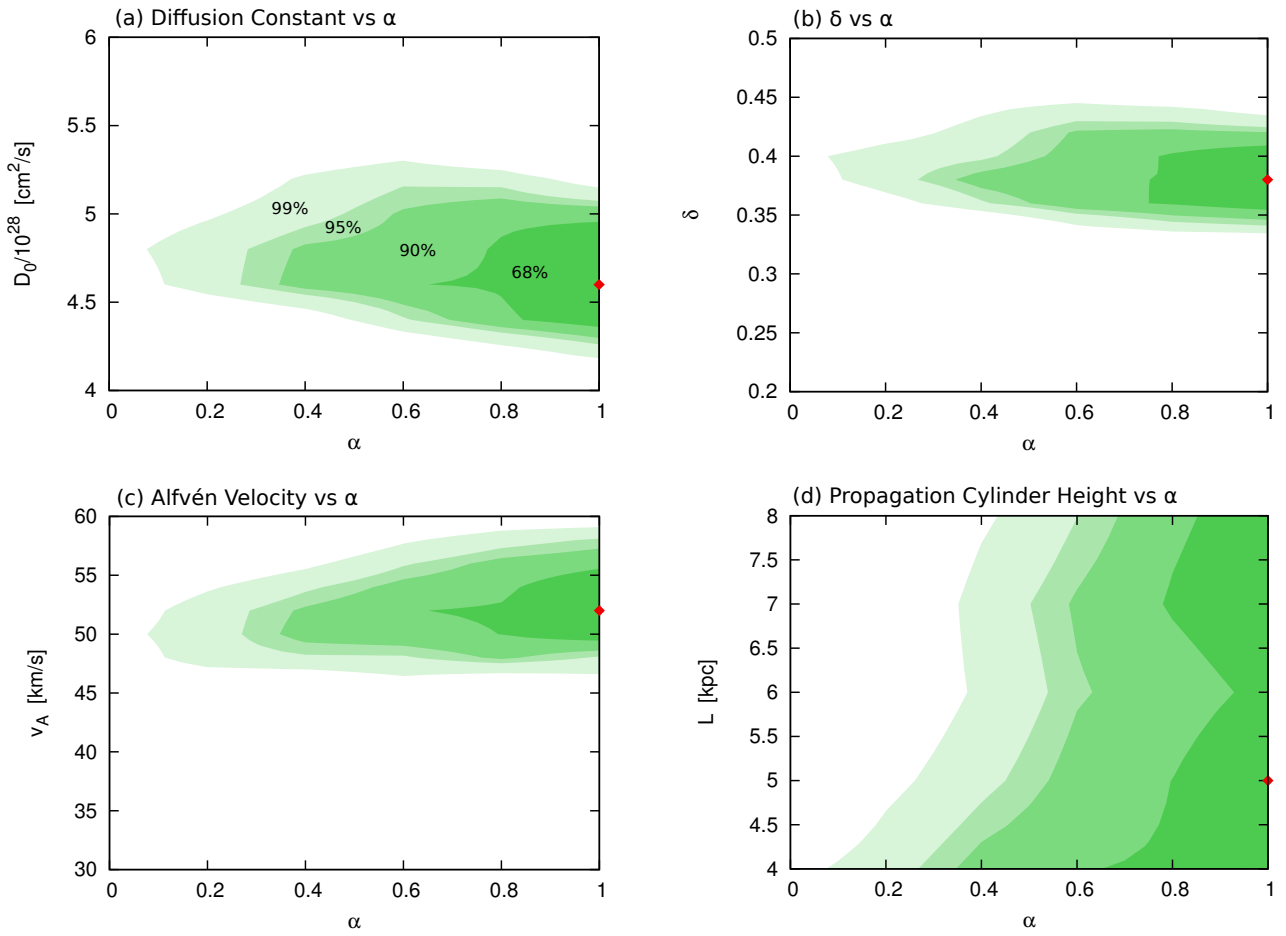


Figure 1: Two-parameter likelihood surfaces for the transport parameters as a function of the diffusion gradient index  $\alpha$ , obtained for combined fit to B/C and  $^{10}\text{Be}/^9\text{Be}$  flux ratios. Contours for  $\Delta\chi^2 = 2.3, 4.61, 5.99,$  and  $9.21$  are given, corresponding to the 68%, 90%, 95% and 99% confidence level regions, respectively. Subfigures: (a) diffusion constant  $D_0$ , (b) diffusion coefficient power index  $\delta$ , (c) Alfvén velocity  $v_A$ , (d) propagation cylinder maximum height  $L$ . The red diamond indicates the location of  $\chi_{\min}^2$ . Whereas isotropic diffusion models with  $\alpha = 0$  ( $D_{xx}$  independent of position) cannot accommodate the high velocity convective winds suggested by ROSAT, models with  $\alpha = 1$  ( $D_{xx} \propto |z|$ ) can give a very good fit.

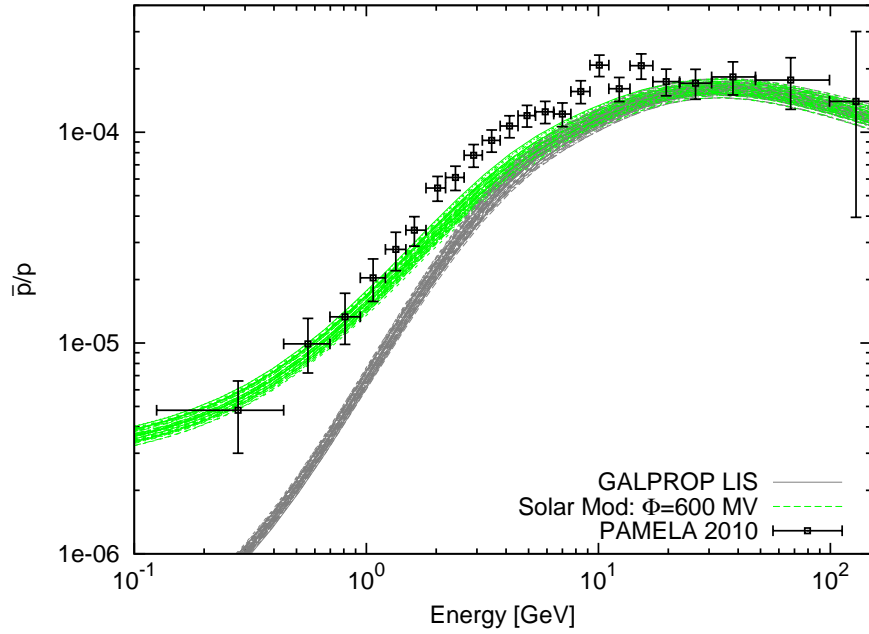
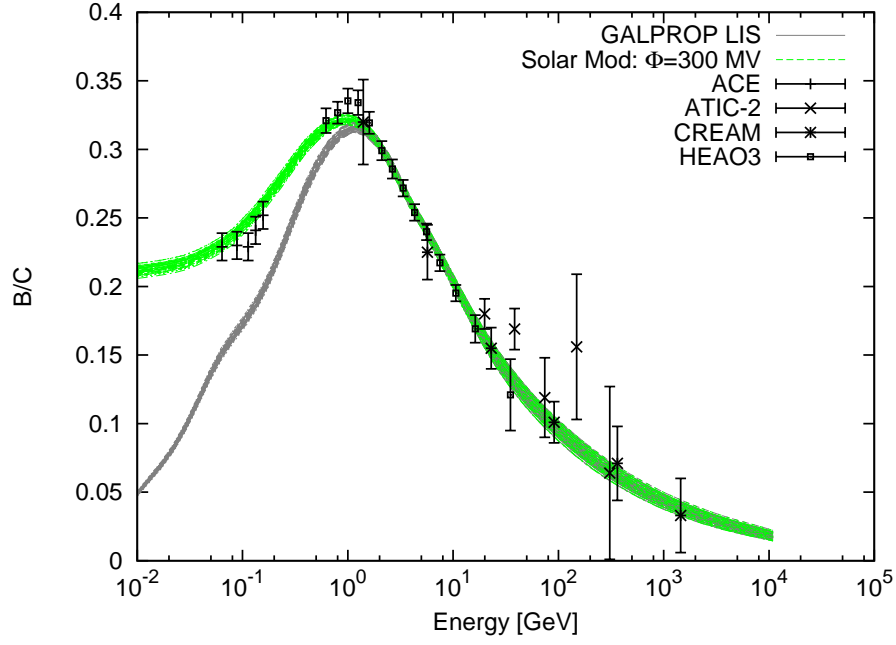


Figure 2: Predicted flux distribution for models within the 68% confidence level region (four parameter fit  $\Delta\chi^2 = 4.72$ ), for the combined fit to B/C and  $^{10}\text{Be}/^9\text{Be}$ . The grey (dark) curves indicate the local interstellar (LIS) flux, while the green (light) curves have been corrected for solar modulation using the “force field” approximation (modulation potential indicated). The B/C flux ratio is reproduced well, however the predicted  $\bar{p}/p$  flux is significantly lower than the PAMELA measurements between approximately 2 GeV to 20 GeV.

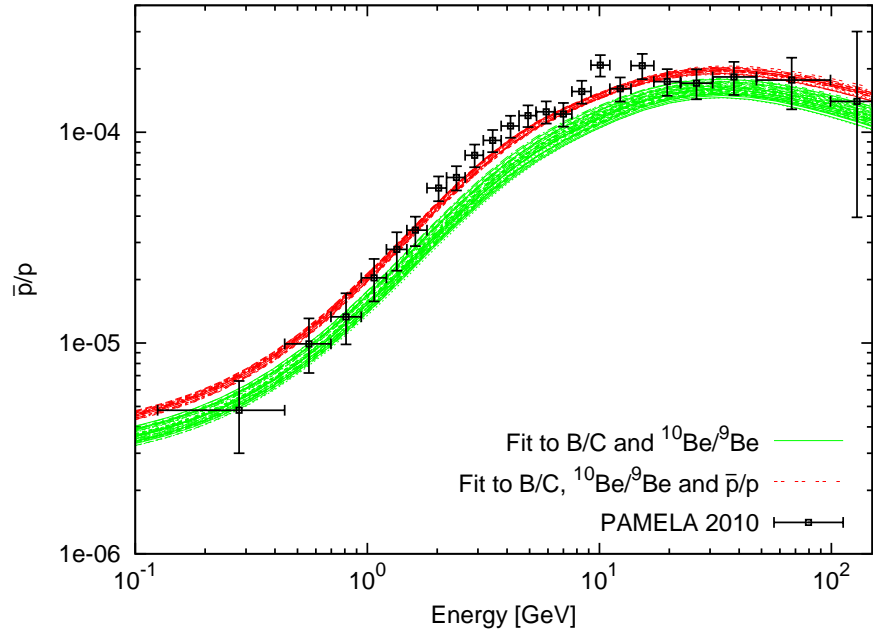
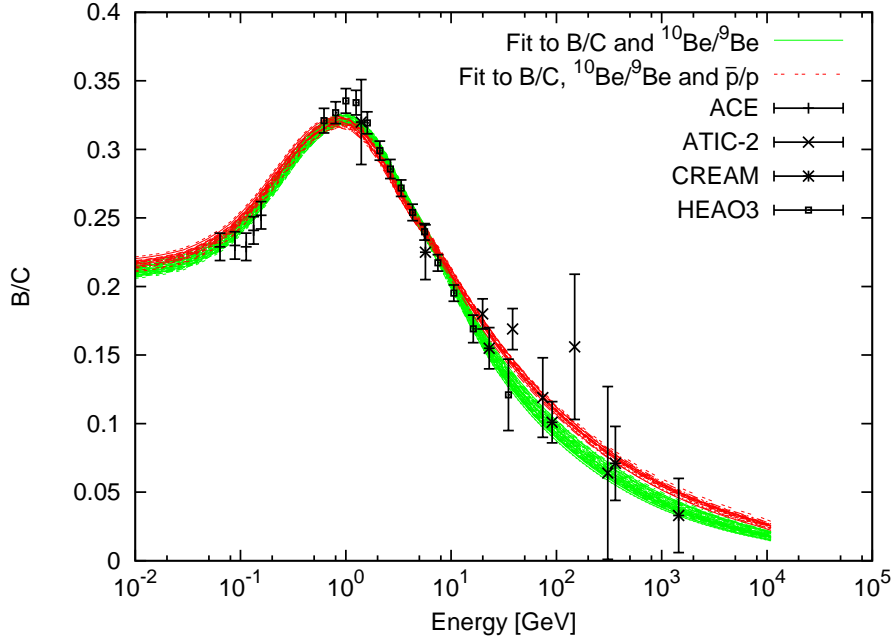


Figure 3: The predicted flux distribution obtained for models within the 68% confidence level region for the combined fit to the B/C,  $^{10}\text{Be}/^9\text{Be}$ , and  $\bar{p}/p$  data in red (dark) superimposed on the results obtained for the fit to B/C and  $^{10}\text{Be}/^9\text{Be}$  only in green (light). The  $\chi^2_{\min}$  is observed to increase by  $\Delta\chi^2 = 35.4$  for the additional 23 PAMELA data points considered. The fit to the B/C flux is degraded as the distribution does not reproduce well the high precision HEAO-3 measurements above 10 GeV. The fit to  $\bar{p}/p$  is marginally improved, however the distribution is still lower than the PAMELA observation between approximately 2 GeV and 15 GeV.

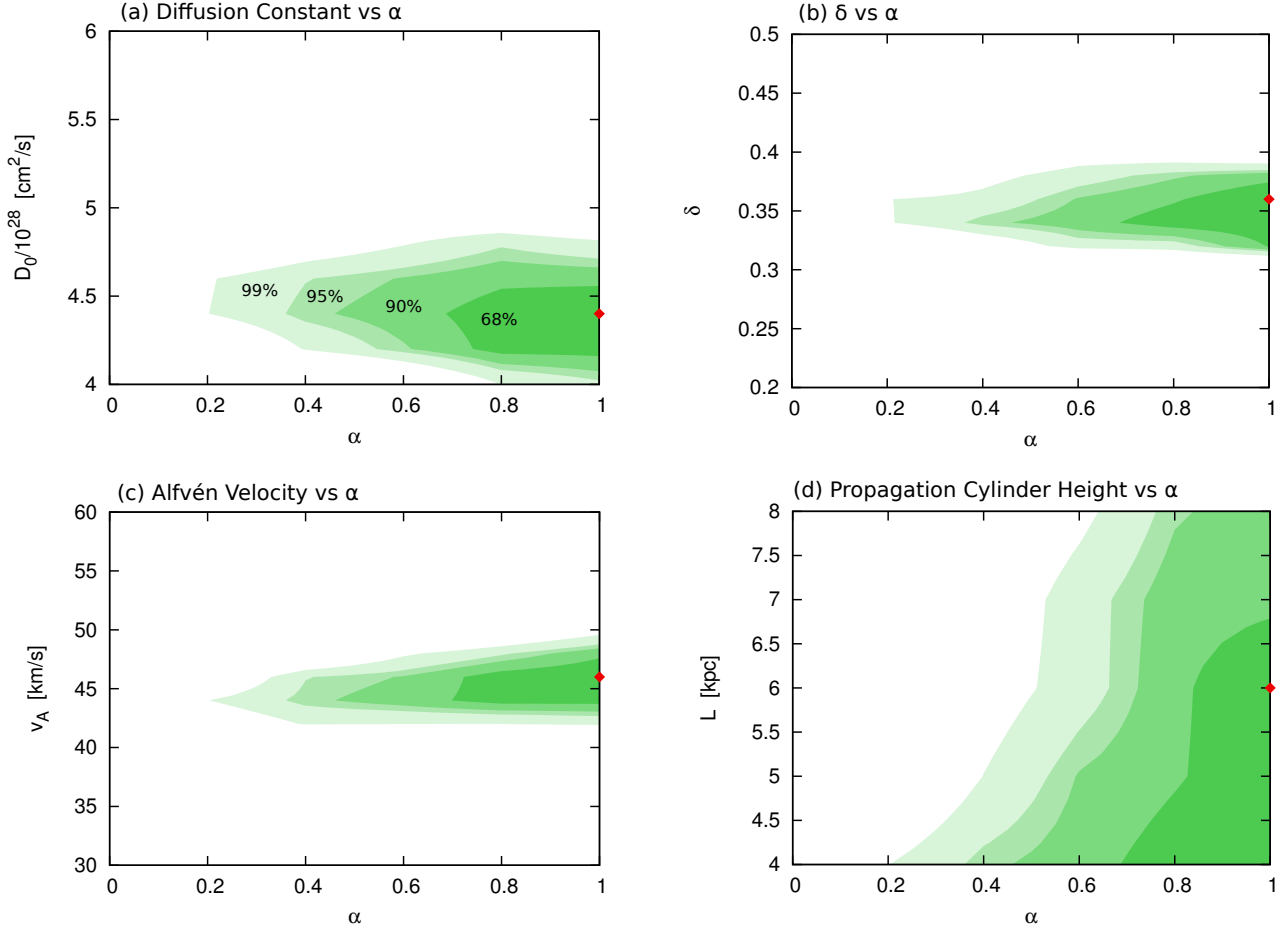


Figure 4: Two-parameter likelihood surfaces for the transport parameters as a function of the diffusion gradient index  $\alpha$ , obtained for combined fit to B/C,  $^{10}\text{Be}/^9\text{Be}$  and  $\bar{p}/p$  flux ratios. The contours are as in Fig. 1. We find an increase of  $\chi^2_{\min}$  by  $\Delta\chi^2 = 35.4$  for the 23 PAMELA data points considered, and a significant reduction of the Alfvén wave velocity ( $v_A$ )